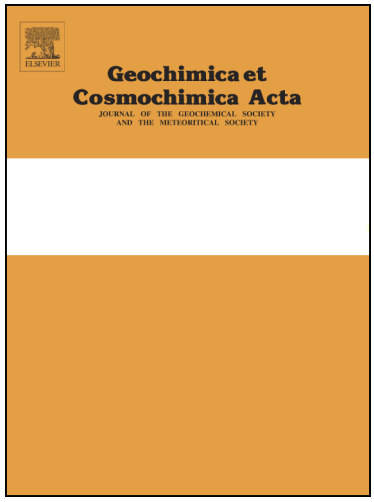

Evaluation of branched GDGTs and leaf wax *n*-alkane δ ^{2}H as (paleo) environmental proxies in East Africa

Sarah Coffinet, Arnaud Huguet, Nikolai Pedentchouk, Laurent Bergonzini, Christine Omuombo, David Williamson, Christelle Anquetil, Martin Jones, Amos Majule, Thomas Wagner, Sylvie Derenne

PII: S0016-7037(16)30662-7
DOI: http://dx.doi.org/10.1016/j.gca.2016.11.020
Reference: GCA 10028

To appear in: *Geochimica et Cosmochimica Acta*

Received Date: 13 April 2016
Revised Date: 8 November 2016
Accepted Date: 12 November 2016

Please cite this article as: Coffinet, S., Huguet, A., Pedentchouk, N., Bergonzini, L., Omuombo, C., Williamson, D., Anquetil, C., Jones, M., Majule, A., Wagner, T., Derenne, S., Evaluation of branched GDGTs and leaf wax *n*-alkane δ ^{2}H as (paleo) environmental proxies in East Africa, *Geochimica et Cosmochimica Acta* (2016), doi: http://dx.doi.org/10.1016/j.gca.2016.11.020

Evaluation of branched GDGTs and leaf wax *n*-alkane δ^2H as (paleo) environmental proxies in East Africa

Sarah Coffinet[a1], Arnaud Huguet[a], Nikolai Pedentchouk[b], Laurent Bergonzini[c], Christine Omuombo[d], David Williamson[e], Christelle Anquetil[a], Martin Jones[f], Amos Majule[g], Thomas Wagner[h], Sylvie Derenne[a]

[a]*Sorbonne Universités, UPMC Univ Paris 06, CNRS, EPHE, UMR 7619 METIS, 4 place Jussieu, 75252 Paris cedex 05, France*
[b]*School of Environmental Sciences, University of East Anglia, Norwich Research Park, Norwich, NR4 7TJ, United Kingdom*
[c]*Université Paris Saclay, UPS Univ Paris 11, CNRS, UMR 8148 GEOPS, rue du belvédère, Bât 504, 91405 Orsay cedex, France*
[d]*Department of Geology, University of Nairobi, Chiromo Campus, P.O. Box 30197, 00100 Nairobi, Kenya*
[e]*Institut de Recherche pour le Développement, Sorbonne Universités, UPMC Univ Paris 06, MNHN, CNRS, UMR 7159 LOCEAN, Centre IRD France Nord, F-93143, Bondy cedex, France*
[f]*Newcastle University, School of Civil Engineering and Geosciences, Newcastle-upon-Tyne, NE1 7RU, United Kingdom*
[g]*Institute of Resource Assessment, University of Dar Es Salaam, P.O. Box 35097, Dar Es Salaam, Tanzania*
[h]*Heriot-Watt University, Lyell Centre for Earth and Marine Science and Technology, School of Energy, Geoscience, Infrastructure and Society (EGIS), Edinburgh, EH14 4AS, United Kingdom*

Corresponding author email address: scoffinet@marum.de ; +49 421 218 65740

Abstract

The role of mountain evolution on local climate is poorly understood and potentially underestimated in climate models. One prominent example is East Africa, which underwent major geodynamic changes with the onset of the East African Rift System (EARS) more than 250 Myr ago. This study explores, at the regional East African scale, a molecular approach for terrestrially-based paleo-climatic reconstructions that takes into account both changes in temperature and in altitude, potentially leading to an

1 Present address: MARUM – Center for Marine Environmental Sciences, University of Bremen, Leobener Str., 28359 Bremen, Germany

34 improved concept in paleo-climatic reconstructions. Using surface soils collected along
35 pronounced altitudinal gradients in Mt. Rungwe (n=40; Southwest Tanzania) and Mt.
36 Kenya (n=20; Central Kenya), we investigate the combination of 2 terrestrial proxies, leaf
37 wax *n*-alkane δ^2H (δ^2H_{wax}) and branched glycerol dialkyl glycerol tetraether (br GDGT)
38 membrane lipids, as (paleo) elevation and (paleo) temperature proxies, respectively. At
39 the mountain scale, a weak link between δ^2H_{wax} and altitude ($R^2 = 0.33$) is observed at
40 Mt. Kenya, but no relationship is observed at Mt. Rungwe. It is likely that additional
41 parameters, such as decreasing relative humidity (RH) or vegetation changes with
42 altitude, are outcompeting the expected ^2H-depletion trend along Mt. Rungwe. In
43 contrast, br GDGT-derived absolute mean annual air temperature (MAAT) and
44 temperature lapse rate (0.65 °C/100 m) for both mountains are in good agreement with
45 direct field measurements, further supporting the robustness of this molecular proxy for
46 (paleo) temperature reconstructions. At the regional scale, estimated and observed δ^2H
47 data in precipitation along 3 mountains in East Africa (Mts. Rungwe, Kenya and
48 Kilimanjaro) highlight a strong spatial heterogeneity, preventing the establishment of a
49 regional based calibration of δ^2H_{wax} for paeloaltitudinal reconstructions. Different from
50 that, an improved regional soil calibration is developed between br GDGT distribution
51 and MAAT by combining the data from this study (Mts. Rungwe and Kenya) with
52 previous results from East African surface soils along Mts. Kilimanjaro (Tanzania) and
53 Rwenzori (Uganda). This new regional calibration, based on 105 samples, improves both
54 the R^2 (0.77) and RMSE (root mean square error; 2.4 °C) of br GDGT-derived MAAT
55 over the global soil calibrations previously established ($R^2 = 0.56$; RMSE = 4.2 °C) and
56 leads to more accurate (paleo) temperature reconstructions in the region.

1. Introduction

The East African Rift System (EARS) is one of the best examples of an active rift system. The initial rifting in the area dates back to the Permo-Triassic and Cretaceous (Macgregor, 2015). The development of this complex system with several phases of rifting dramatically changed the East African landscape. Yet its potential influence on the vegetation and local and African climate is hardly constrained. Previous modelling (Sepulchre et al., 2006) postulated that the rise of the EARS should have greatly contributed to the long term aridification of East Africa. However, these simulations only compared 2 extreme scenarios: (i) no elevation and (ii) high elevation – reflecting the lack of a well constrained history of the EARS rise. Moreover, paleo-climate reconstructions in East Africa have long been hampered by 2 challenges: (i) traditional hydrological proxies, such as lake level studies, are influenced not only by changes in the amount of precipitation but also by ambient temperature; (ii) temperature changes are poorly constrained because few sedimentary proxies are sensitive enough to accurately record the small scale temperature variations in tropical lakes (*Verschuren et al., 2009*).

Recently, novel proxies were developed based on the analysis of fossil organic compounds containing environmental information in their structures. Notably, leaf wax *n*-alkane δ^2H (δ^2H_{wax}) was proposed as a (paleo) elevation proxy (Jia et al., 2008) while branched glycerol dialkyl glycerol tetraether (br GDGT) membrane lipids are increasingly used as a (paleo) temperature proxy (Weijers et al., 2007). The combined use of these 2 proxies could thus help to better constrain the relationships between topography and climate in East Africa.

Long chain *n*-alkanes are produced primarily by higher terrestrial plants (Eglinton and Hamilton, 1967) and their $^{2}H/^{1}H$ ratio, typically expressed as $\delta^{2}H_{wax}$, is linked with the $^{2}H/^{1}H$ ratio of the plant water source (e.g. Sauer et al., 2001). Because *n*-alkanes are well preserved in the geological archives (Eglinton and Eglinton, 2008) and their hydrogen not easily exchangeable (Schimmelmann et al., 2006), the $\delta^{2}H_{wax}$ is frequently used in paleo-climate studies to track the variability of the $^{2}H/^{1}H$ ratio of meteoric water ($\delta^{2}H_{p}$), as recently reviewed by Sachse et al. (2012). The 'altitude effect', described by Dansgaard (1964), is one of the physical parameters impacting the $\delta^{2}H_{p}$ and it corresponds to the progressive ^{2}H-depletion of precipitation along altitudinal gradients due to successive Rayleigh distillation equilibria as the air mass rises. This effect has been observed in precipitation along several mountains across the world (Araguás-Araguás et al., 2000) including 2 equatorial African mountains: Mt. Cameroon (Cameroon; Gonfiantini et al., 2001) and Mt. Kilimanjaro (Tanzania; Zech et al., 2015). The ability of $\delta^{2}H_{wax}$ to track this altitudinal effect was first shown at Mt. Gongga (China; Jia et al., 2008). This relationship was further observed at several mountains in Asia, Oceania and America (e.g. Luo et al., 2011; Ernst et al., 2013; Bai et al., 2015; Zhuang et al., 2015).

Branched GDGTs represent another group of biomarkers increasingly used for paleo-climate reconstructions in terrestrial archives (e.g. Peterse et al., 2011). These membrane lipids (Suppl. Fig.) are ubiquitous in both terrestrial and aquatic environments (Schouten et al., 2013) and are produced by yet unknown bacteria. In soils from across the globe, the relative abundance of the different br GDGTs was shown to depend on environmental parameters (Weijers et al., 2007), leading to the development of global

103 calibrations between br GDGT distribution and mean annual air temperature (MAAT)
104 and pH (Weijers et al., 2007; Peterse et al., 2012). These compounds can therefore be
105 used as paleo-thermometers. Soil-derived br GDGTs have been investigated along
106 several mountain transects (e.g.; Peterse et al., 2009; Ernst et al., 2013; Anderson et al.,
107 2014) with a high variability in temperature (as temperature decreases with altitude). In
108 the previously published papers, the related br GDGT-derived MAAT were found to (i)
109 be in agreement with local measured MAAT and (ii) relate with altitude (i.e. following
110 the natural temperature gradient), even though a high degree of scatter was observed for
111 some case studies (e.g. Mt. Gongga; Peterse et al., 2009).

112 The combination of δ^2H_{wax} and br GDGT provided promising results which
113 significantly expand their potential for (paleo) climate reconstruction. In modern soils,
114 they were found to both correlate with altitude along Mt. Gongga (China, Jia et al., 2008
115 and Peterse et al., 2009), Mt. Meghalaya (India, Ernst et al., 2013) and the Southern Alps
116 (New Zealand, Zhuang et al., 2015) implying that δ^2H_{wax} was recording the altitude effect
117 in δ^2H_p and br GDGTs the natural temperature gradient. In geological archives, the
118 approach has been employed to reconstruct the early Eocene elevation and climatic
119 history of the Sierra Nevada (Hren et al., 2010). It was deduced from the analysis of
120 δ^2H_{wax} from fossil leaves and br GDGTs from the sediment matrix that, during the
121 Eocene Climatic Optimum, Sierra Nevada elevation was high (> 2 km) with warmer air
122 temperature than today. In East Africa, however, altitudinal transects from the southern
123 slope of Mt. Kilimanjaro (Tanzania) was investigated by several groups (Sinninghe
124 Damsté et al., 2008; Peterse et al., 2009; Zech et al., 2015), resulting in inconsistent
125 results. While estimated air temperatures derived from the analysis of br GDGTs were

consistent with the observational temperature data (Sinninghe Damsté et al., 2008), no clear altitudinal trend was observed for δ^2H_{wax} (Peterse et al., 2009; Zech et al., 2015). This prompts the question regarding the relative importance of site (mountain)-related and regional (East African)-related controls on the link between altitude and soil δ^2H_{wax} record.

In the present study, δ^2H_{wax} and br GDGTs were analysed in 60 surface soils along 2 East African mountains – Mt. Rungwe (n=40; Southwest Tanzania; Fig. 1) and Mt. Kenya (n=20; Central Kenya; Fig. 1) – to further test their joint applicability as (paleo) environmental proxies in this climatically sensitive area. Our results were then combined with previously published data for 2 additional East African mountains (Mt. Rwenzori, Uganda, Loomis et al., 2011; Mt. Kilimanjaro, Tanzania, Peterse et al., 2009, Sinninghe Damsté et al., 2008 and Zech et al., 2015) to potentially generate regional calibrations of δ^2H_{wax} variations with elevation and br GDGT variations with temperature. This could improve the precision/quality of regional scale (paleo) elevation and (paleo) temperature reconstructions in comparison with global calibrations. The ultimate goal of this work is to introduce improved tools for terrestrially-based paleo-climatic reconstructions in East Africa that take into account not only temperature but also altitude changes, and which could then be used to reconstruct the evolution of topography and climate dynamics over geological time in the EARS.

2. Materials and Methods

2.1. Study sites

Br GDGTs and *n*-alkanes were analysed in 40 surface soils collected between 500 and 2800 m along the gentle then steep slope of Mt. Rungwe in 2012 and 2014, and in 20 samples collected between 1900 and 3300 m along the steady gentle slope of Mt. Kenya in 2013 (Table 1). About 50-60 g of soil were collected in the A horizon (0-5 cm) and kept at room temperature before shipping to France by plane.

Mt. Rungwe is located in the Southwest of Tanzania (9° S, 33° E; Fig. 1) and experiences a typical tropical climate, with alternations between a hot and humid (from November to May) season and a colder and drier season (from June to October; Delalande et al., 2008). Natural vegetation along the altitudinal transect belongs to the Zambezian Miombo-type woodland at low altitude and Afromontane vegetation at higher altitude (e.g. Vincens et al., 2003). Agriculture – including banana, rice, cocoa, tea, coffee, maize cultivations – is practiced up to 1500 m leading to partial deforestation of the mountain slopes (Williamson et al., 2014). MAAT was continuously measured with temperature loggers (weather station, DAVIS, Instruments, Hayward, CA, USA) at 540 m, 920 m and 1720 m and varied from 25.6 °C at 540 m to 22.6 °C at 920 m and 16.9 °C at 1720 m, leading to a temperature gradient of 0.7 °C/100 m.

Mt. Kenya is the highest mountain in Kenya (5199 m.a.s.l.) and is located on the equator (0° S 37° E; Fig. 1). The twice-yearly passage of the Intertropical Convergence Zone (ITCZ) leads to a bimodal rainfall pattern characterized by the onset and duration of the long rains (March to May) and short rains (October to November), the other months experiencing a drier climate (Camberlin et al., 2014). Present day vegetation is marked by

five distinguishable altitudinal zones, (Bremond et al., 2008; Hamilton, 1982) from the mountain forest belt at its base (1960–2500 m.a.s.l.) to Afroalpine at its top (3400–4200 m.a.s.l.), with Bamboo and Ericaceous zones in between. Based on meteorological data from weather stations along Mt. Kenya and in Central Kenya (Camberlin et al., 2014; Kenya Meteorological Department, 1984; Kenya Meteorological Department; Smith, 1993), temperature lapse rate along Mount Kenya was determined as 0.63 °C/100 m.

2.2. Sample preparation

Samples were frozen and freeze-dried at their arrival in Paris (France) and then kept at -18 °C prior further treatment. Sample preparation was identical to that detailed by Coffinet et al. (2014). Briefly, soils were extracted (3 × 5 min) with dichloromethane (DCM): methanol (MeOH) (9:1, v:v) using an accelerated solvent extractor (ASE 100 – Dionex; 100°C, 10×10^6 Pa). The extract was separated into 2 fractions through a 2 cm diam. column of Al_2O_3 (activated overnight at 150 °C) using heptane:DCM (9:1, v:v) and DCM:MeOH (1:1, v:v) respectively. The 2 fractions were then rotary evaporated, re-dissolved in 1 ml heptane and centrifuged using an Eppendorf Mini Spin centrifuge (1 min, 7000 rpm) prior to further analysis.

2.3. n-Alkane analysis

n-Alkanes were analysed at UPMC, Paris, France by gas chromatography coupled to a mass spectrometer (GC-MS) using an Agilent Network 6890 GC System coupled with a 5973 Mass Selective Detector, with electron impact at 70eV. 1 µl was injected and

194 the separation was achieved using a Restek RXI-5 Sil MS silica capillary column (30 m ×
195 0.25 mm i.d., 0.50 µm film thickness) with He as the carrier gas at 1 ml/min flow rate.
196 The GC oven initial temperature was set to 50 °C and then increased to 320 °C at a 4
197 °C/min. Samples were injected in splitless mode and the injector temperature was 280 °C.
198 *n*-Alkane hydrogen isotopic composition was measured at Newcastle University,
199 UK using a Delta V+ isotope-ratio mass spectrometer (IRMS, ThermoFisher) connected
200 to a GC Ultra Trace (ThermoFisher), a Finnigan GC Combustion III (ThermoFisher) and
201 a high temperature conversion (HTC) system set up at 1400 °C. The GC oven initial
202 temperature was set to 50 °C and then increased to 250 °C at 15 °C/min and from 250 °C
203 to 320 °C at 5 °C/min. The GC oven was held at 320 °C for 15 min. Every sample was
204 analysed in duplicate and the $^{2}H/^{1}H$ ratio was reported on the VSMOW (Vienna standard
205 mean ocean water) scale to determine compound specific $\delta^{2}H_{Cn}$ (‰). The H_3 factor was
206 measured daily and varied between 2.48 and 2.61 during the course of analysis.
207 Sample *n*-alkane δ²H values were corrected individually using an *n*-alkane standard (*n*-
208 C16 to *n*-C30; mix A5) and 5α-androstane standard (A. Schimmelmann, Indiana
209 University), run at the beginning and at the end of each sample sequence. Standard error
210 of the measurements of the long chain *n*-alkanes (C_{25}-C_{31}) from this standard mix ranged
211 between 0.3‰ and 1.1‰.

212

213 2.4. Br GDGT analysis

214 Br GDGT analysis was performed at UPMC, Paris, France by high pressure liquid
215 chromatography coupled to a mass spectrometer with an atmospheric pressure chemical
216 ionization source (HPLC-APCI-MS). Samples from Mt. Rungwe collected in 2014 were

217 analysed with a Shimadzu LCMS-2020, as described by Coffinet et al. (2015), whereas
218 samples from Mt. Kenya and those from Mt. Rungwe collected in 2012 were analysed
219 with an Agilent 1100 series HPLC instrument equipped with an automatic injector and
220 coupled to a PE Sciex API 3000 mass spectrometer, using a procedure described by
221 Coffinet et al. (2014). Similar chromatographic conditions were used on the 2 machines
222 and samples from Coffinet et al. (2014) were re-run with the Shimadzu LCMS-2020 to
223 assess the method reproducibility between the 2 LCMS apparatus (mean errors: 0.03 for
224 MBT, 0.05 for CBT and 0.28 °C for MAAT).

225 Semi-quantification of br GDGTs was performed by comparing the integrated
226 signal of the respective compound with the signal of a C_{46} synthesised internal standard
227 (Huguet et al., 2006) assuming their response factors to be identical.

228 The MBT' (methylation index of branched tetraethers; eq. 1; Peterse et al., 2012)
229 and CBT (cyclisation ratio of branched tetraethers; eq. 2; Weijers et al., 2007) indices
230 were determined from the following equations:

231 $$MBT' = \frac{[Ia + Ib + Ic]}{[IIIa] + [IIa + IIb + IIc] + [Ia + Ib + Ic]} \quad (1)$$

232 $$CBT = -\log\left(\frac{[IIb] + [Ib]}{[IIa] + [Ia]}\right) \quad (2)$$

233 Roman numerals refer to the structures in the Supplementary Figure.

234 Based on triplicate injections, the maximal analytical error for the different indices was:
235 0.09 for MBT' and 0.03 for CBT.

MAAT was estimated from the global soil calibration developed by Peterse et al., (2012; Eq. 3):

$$MAAT = 0.81 - 5.67 \times CBT + 31.0 \times MBT' \quad (3)$$

2.5. Estimation of the H isotopic composition of precipitation

To characterize the H isotope composition of precipitation (δ^2H_p) at the studied sites, results from previous publications were gathered (Rieti-Shati et al., 2010; Nivet et al., 2015; Zech et al., 2015). Due to the limited number of instrumental data, δ^2H_p was also estimated with the Online Isotopes in Precipitation Calculator (OIPC; Bowen, 2016; Bowen and Revenaugh, 2003). The OIPC model was developed to allow point estimation of δ^2H_p. It is based on a spatial interpolation from the 340 Global Network for Isotope in Precipitation (GNIP) station database. This interpolation includes the latitude and altitude effects on the isotopic composition of precipitation but in some regions, including East Africa, it is limited by additional sources of uncertainty. In East Africa, the major source of uncertainty is the small number of GNIP stations which lowers the dataset resolution (Bowen and Revenaugh, 2003; West et al., 2004) while the δ^2H_p variability is there especially high (due to the intertropical context and the orographic complexity). In addition, Bowen and Wilkinson (2002) pointed out 2 high altitude stations (Addis-Abeba and Entebbe) where the measured isotopic composition of precipitation was anomalously enriched in heavy isotopes, leading to an increased uncertainty in the prediction of δ^2H_p in this region. For the estimations along the 3 studied mountains, the 95% confidence level of the model varied from 3-4‰ at low altitudes to 6‰ at higher altitudes.

3. Results

3.1. δ^2H_p and δ^2H_{wax} along the altitudinal transects at Mt. Kenya and Mt. Rungwe

The δ^2H_p values along Mts. Kenya, Rungwe and Kilimanjaro obtained using the OIPC (the Online Isotopes in Precipitation Calculator; Bowen, 2016; Bowen and Revenaugh, 2003; Fig. 2) span from -42‰ at 3270 m.a.s.l. to -23‰ at 1900 m.a.s.l. along Mt. Kenya and from -49‰ at 2800 m.a.s.l. to -16‰ at 520 m.a.s.l. along Mt. Rungwe and from -45‰ at 3245 m.a.s.l. to -23‰ at 1727 m.a.s.l along Mt. Kilimanjaro.

n-Alkanes were analysed in 20 soil samples collected between 1900 to 3160 m along Mt. Kenya and in 40 soil samples collected between 500 and 2800 m along Mt. Rungwe. The distribution parameters of these compounds (chain length range, C_n range; average chain length, ACL; carbon preference index, CPI; cf. Supplementary Table 1) do not show any statistically relevant correlation with altitude. Along the two transects, long chain *n*-alkanes with odd-over-even predominance were the most abundant, as reflected by overall high ACL (28 ± 2; Suppl. Table 1) and CPI values (between 3 and 18; Suppl. Table 1). These results indicate that *n*-alkanes present in the soils originate predominantly from higher plants. The δ^2H values are comprised between -109‰ and -177‰ (mean -143‰) at Mt. Rungwe, and between -116‰ and -167‰ at Mt. Kenya (mean -141‰; Suppl. Table 1). The weighted mean δ^2H_{wax} of the long chain *n*-alkanes (C_{27}, C_{29}, C_{31}) varied between -166‰ and -125‰ (Table 1) along Mt. Rungwe and between -158‰ and -119‰ along the slope at Mt. Kenya.

3.2. Br GDGT-derived mean annual air temperature (MAAT) along the altitudinal transects at Mts. Rungwe and Kenya

Br GDGTs were analysed along Mt. Kenya in the same soil samples as those analysed for *n*-alkanes (n=20). Br GDGT proxies and corresponding temperature estimates were previously determined in 20 surface soils collected at Mt. Rungwe in 2012 (Coffinet et al., 2014). This dataset was extended in the present study by the analysis of br GDGTs in 16 additional soil samples (same sample set as for the *n*-alkane analysis except 3 of them which were not analysed, see details in Table 1) collected along Mt. Rungwe. The distribution of br GDGTs was similar in soils collected in 2012 and 2014, as shown by the comparable ranges of MBT' and CBT values in these samples (cf. Suppl. Table 2).

Br GDGT-derived MAATs were estimated using the global soil calibration (Peterse et al., 2012) and varied from 9.3 °C at 3270 m.a.s.l. to 16.9 °C at 1900 m.a.s.l. along Mt. Kenya and from 12.2 °C at 2055 m.a.s.l. to 22.5 °C at 529 m.a.s.l. (Table 1).

4. Discussion

4.1. Variation of δ^2H of *n*-alkanes in East Africa

In East Africa, the altitude effect on the hydrogen isotopic ratio of precipitation (δ^2H_p) was reported along Mt. Kilimanjaro above 2000 m.a.s.l. (1.4‰/100 m) while it tends to be much weaker at lower altitudes (Zech et al., 2015 and Fig. 2). As Gonfiantini et al. (2001) observed at Mt. Cameroon (Cameroon), the altitudinal gradient in the δ^2H_p seems to increase with altitude. Along Mt. Rungwe, the establishment of a long term

monitoring of the isotopic composition of precipitation is ongoing (Nivet et al., 2015). Preliminary data indicate values ranging from -16.9‰ at 1720 m.a.s.l. to -12.9‰ at 920 m.a.s.l. and -11.3‰ at 540 m.a.s.l. (Fig. 2) but more data are needed at higher altitudes to compare with Mts. Kilimanjaro and Cameroon trends. Along Mt. Kenya, Rieti-Shati et al. (2000) suggested the altitude effect to be absent based on precipitation events collected between 3000 and 4000 m.a.s.l. and groundwater collection above 4500 m.a.s.l. However this assumption is based on a very limited dataset from high altitude sampling sites on the western side of the mountain whereas sampling for the present study was performed on the North-East slope of Mt. Kenya. Long-term monitoring of precipitation along a wide elevation range of this slope side at Mt. Kenya is needed to precisely assess the variation of its isotopic composition.

Because of this limited number of measured isotopic values of precipitation along the studied mountains, δ^2H_p had to be estimated using the OIPC (the Online Isotopes in Precipitation Calculator; Bowen, 2016; Bowen and Revenaugh, 2003; Fig. 2). A ^2H-depletion lapse rate of 1.5 ‰/100 m was computed for Mts. Rungwe and Kenya and of 1.4‰/100 m for Mt. Kilimanjaro, similar to the one measured by Zech et al. (2015) above 2000 m.a.s.l. (Fig. 2). Nevertheless, along the latter, the OIPC data were observed to be shifted from the measured ones, particularly at higher altitudes, towards more depleted values and to a higher extent than the 95% confidence level estimated by the model (ca. 11‰ difference; Fig. 2). Such a shift was already observed and discussed in Kenya by Soderberg et al. (2013) and is likely due to the low number of GNIP stations whilst the rain composition exhibits a high spatial variability in the region. Therefore the absolute values derived from the OIPC must be treated with caution. However, they

328 should depict the likely trend of δ^2H_p related to the altitude effect and allow comparison
329 between the three studied sites. Notably, the δ^2H_p varies from one mountain to another
330 (Fig. 2). At a given altitude, 870 m.a.s.l. for example, δ^2H_p equals -22‰, -12‰, -8‰
331 along Mts. Rungwe, Kilimanjaro and Kenya, respectively. More specifically, the more
332 northern the latitude, the more enriched the δ^2H_p. This illustrates that, in addition to
333 altitude, a latitudinal effect is also likely to impact the δ^2H_p distribution in East Africa, as
334 previously noted at the global scale by Dansgaard (1964). No calibration of δ^2H_p with
335 altitude could thus be deduced at the regional, East African, scale and the altitudinal
336 effect in δ^2H_p could only be tracked at the mountain scale. Consequently, in the
337 following, the ability of δ^2H of *n*-alkanes (δ^2H_{wax}) to track the altitudinal effect on δ^2H_p
338 was solely investigated at the mountain scale for each study site.

339 The concentration-weighted mean values of δ^2H $C_{27} - C_{31}$ alkanes (δ^2H_{wax}, Table
340 1) were plotted against altitude for Mt. Kenya and Mt. Rungwe (Fig. 3A-B). A
341 statistically significant, though scattered, ^2H-depletion trend was observed along Mt.
342 Kenya (-1.2‰/100 m; Fig. 3A; $p < 0.05$) close to the gradient observed for precipitation
343 along Mt. Kilimanjaro (-1.4‰/100 m, Fig. 2). This result indirectly suggests the
344 existence of an altitude effect in δ^2H_p along Mt. Kenya, unlike what was previously
345 reported by Rieti-Shati et al. (2000). The δ^2H_{wax} values along Mt. Kenya support the
346 hypothesis that *n*-alkanes are able to record the altitude effect in their $^2H/^1H$ ratio,
347 consistent with evidence from several other mountain systems in Asia (e.g. Jia et al.,
348 2008; Bai et al., 2015) and New Zealand (Zhuang et al., 2015). In contrast, no trend was
349 noticed at Mt. Rungwe (Fig. 3B, $p > 0.05$), as previously observed along Mt. Kilimanjaro
350 (Peterse et al., 2009; Zech et al., 2015).

For these two mountains (Rungwe and Kilimanjaro), we suggest that the altitude effect observed in the precipitation may have been overprinted during the biosynthesis of *n*-alkanes and/or their diagenetic reworking in the soil. As reviewed by Sachse et al. (2012), lipid biosynthesis comprises several steps where $^{2}H/^{1}H$ fractionation can occur. The magnitude of fractionation on the end-product $\delta^{2}H_{wax}$ signal is still poorly constrained for most plant species. Notably, Sachse et al. (2012) highlighted several parameters that could have a high impact on the $\delta^{2}H_{wax}$ fractionation, such as vegetation changes, deposition processes and leaf physiology. Several studies pointed out large variability in the leaf-derived $\delta^{2}H_{wax}$ of different species within a same site (e.g. Chikaraishi and Naraoka, 2007; Pedentchouk et al., 2008). Thus, the important vegetation changes with altitude documented along Mts. Kilimanjaro and Rungwe (Bremond et al., 2008; Williamson et al., 2014) could have influenced the $\delta^{2}H_{wax}$ signal, leading to an overprinting of the altitude effect on the $\delta^{2}H$ of the precipitation. Moreover, Zech et al. (2015) postulated that along Mt. Kilimanjaro the altitudinal effect should be outcompeted by the increasing evaporative ^{2}H-enrichment of the leaf water due to changes in humidity with increasing altitude. The impact of these potential additional effects could be enhanced in East Africa, where the altitude effects on $\delta^{2}H_{p}$ (Fig. 2) are in the lower range of the gradients measured across the world (between -1 and -4‰/100 m, Araguás-Araguás et al., 2000).

The results from this study highlight the complexity of the H isotopic signal recorded in *n*-alkanes from East African soils. The altitude effect on $\delta^{2}H_{p}$ was recorded in the $\delta^{2}H_{wax}$ signal at only one altitudinal transect (Mt. Kenya). This suggests that the use of $\delta^{2}H_{wax}$ as a (paleo) elevation proxy might be site-dependent. This study also points to

374 the competitive impact of different hydroclimatic and biogeochemical factors on the soil
375 δ^2H_{wax} record. Unfortunately the lack of extensive environmental monitoring in these
376 remote locations prevented us from determining which of these factors are overprinting
377 the δ^2H_{wax} signal at the other two mountains. Notably, more instrmental data are needed
378 to improve the estimation of the δ^2H_p in East Africa. These observations probably also
379 hold for other mountainous regions across the world and should therefore be taken into
380 consideration in regional scale (paleo) elevation studies. The application of δ^2H_{wax} for
381 (paleo) elevation reconstructions must therefore be limited to the mountain scale and
382 should always be accompanied by detailed surveys of the environmental setting of the
383 study site.
384
385 4.2. East African regional br GDGT calibration
386 Linear altitudinal gradients of measured mean annual air temperatures (MAAT)
387 were observed along all the investigated East African mountains: 0.56 °C/100 m in Mt.
388 Kilimanjaro (Tanzania, Sinninghe Damsté et al., 2008),, 0.53 °C/100 m in Mt. Rwenzori
389 (Uganda, Loomis et al., 2011), 0.73 °C/100 m in Mt. Rungwe (Tanzania, Coffinet et al.,
390 2014, Williamson et al., 2014) and 0.63 °C/100 m in Mt. Kenya (Kenya, Camberlin et al.,
391 2014; Kenya Meteorological Department, 1984; Kenya Meteorological Department;
392 Smith, 1993). The goal of this study was to investigate whether it is possible to establish
393 a regional East African framework for the use of soil derived-br GDGTs as a paleo-
394 thermometer. Thus, the measured MAAT data from all the local East African transects
395 mentioned above were combined to calculate a regional temperature lapse rate (Fig. 4).
396 This rate, determined as 0.65 °C/100 m, with 97% of the MAAT variance being

397 explained by altitudinal variations (Fig. 4), is similar to the one commonly used in low
398 precision studies (Rolland, 2003; Grab, 2013 and references therein) and will allow us to
399 assess the effect of temperature changes on br GDGT distribution at the regional scale.
400 In addition to Mts. Kenya and Rungwe investigated in the present study, br
401 GDGT distribution was previously investigated along two additional East African
402 mountains, Mt. Rwenzori (Uganda; Loomis et al., 2011) and Mt. Kilimanjaro (Tanzania,
403 Sinninghe Damsté et al., 2008). Br GDGT-derived MAATs were estimated using the
404 global soil calibration (Peterse et al., 2012; Weijers et al., 2007) and were found to
405 successfully record the decrease in MAAT with altitude along the slopes of these two
406 previously studied mountains. However, the soils sampled at the highest elevations in Mt.
407 Rwenzori exhibited a significant cold bias (Loomis et al., 2011). The authors suggested
408 that the water saturation of these soils may additionally impact the br GDGT distribution.
409 An impact of extreme soil water content (either aridity or saturation) on br GDGT
410 distribution and corresponding temperature estimates has indeed been reported in several
411 publications (e.g. Huguet et al., 2010 Dirghangi et al., 2013; Menges et al. 2014; Dang et
412 al., 2016).
413 Br GDGT-derived MAATs calculated using the soil calibration by Peterse et al.
414 (2012) were also shown to decrease linearly with altitude along Mts. Rungwe and Kenya
415 (R^2 = 0.79 and 0.66 respectively; figures not shown). Combined together, these four
416 studies highlight the robustness of br GDGTs as a paleo-temperature proxy, at least for
417 East Africa (MAAT lapse-rate = 0.4 °C/100 m, R^2 = 0.63; Fig. 5C). Despite this positive
418 assessment, the application of the global soil calibration still leads to a substantial

419 uncertainty in temperature reconstruction (Root Mean Square Error (RMSE) = 4.2 °C,
420 Peterse et al., 2012; $R^2 = 0.56$, Fig. 5A).

421 Combination of the new and previously published (Sinninghe Damsté et al., 2008;
422 Loomis et al., 2011; Coffinet et al., 2014) data from East Africa, leads to a br GDGT
423 dataset from in total 105 soils. Because of the potential additional impact of water
424 saturation on brGDGT distribution and thus associated temperature estimates, the high
425 elevation samples from Loomis et al. (2011) were not used in this dataset. Based on this
426 integrated sample set, a least square multiple linear regression was performed between br
427 GDGT distribution (MBT' and CBT indices) and the available MAAT for the four sites
428 (Mt. Kenya, Rwenzori, Kilimanjaro and Rungwe). The following equation was obtained:

429 $$MAAT = -8.76 \times CBT + 24.24 \times MBT' + 9.60 \quad (R^2 = 0.77, \text{RMSE} = 2.4\ °C) \quad (4)$$

430 This regional soil calibration (Fig. 5B) strongly improves both the R^2 and RMSE
431 of br GDGT-reconstructed MAAT over the global soil calibration derived from globally
432 distributed soils (Fig. 5A, Peterse et al., 2012). The new East African calibration
433 produces robust quantitative temperatures from br GDGT distributions in soils as it takes
434 into account the regional specificities in soil water content, soil type, biome type, all of
435 which that could potentially impact br GDGT abundance and distribution (e.g. Dirghangi
436 et al., 2013; Menges et al., 2014). This highlights the necessity for regional
437 determinations of the relationship between temperature and br GDGT distribution in
438 order to improve past-temperature estimates. But it also points to the question of defining
439 coherent regions over the globe with a relevant scale.

440 The East African soil calibration developed in this study was applied to the
441 MAAT reconstruction in modern soils along all four altitudinal transects (Fig. 5D). The

resultant br GDGT-derived MAAT lapse rate (0.52 °C/100 m; Fig. 5D) is closer to the measured one (0.65 °C/100 m; Fig. 5D) than when using the global soil calibration (0.41 °C/100 m; 5C), but still underestimates the actual lapse rate by ca. 20 %. This points to the unsuitability of using br GDGTs alone to reconstruct past elevation changes. Independently of that, the correlation between MAAT estimates and altitude is higher when using the new regional soil calibration (R^2 = 0.80; Fig. 5D) than the global one (R^2 = 0.63; Fig. 5C), and closer to the correlation found between instrumental MAAT and altitude (R^2 = 0.97; Fig. 4).. Therefore, the consistency and increase in quality of this new regional calibration for temperature reconstruction calls for its wider application in paleosol-based paleo-climatic reconstructions in East Africa. So far, in this region, br GDGT-derived proxies have only been used in lacustrine sedimentary records (e.g. Tierney et al., 2010; Sinninghe Damsté et al., 2012). This regional but valuable climatic information can also be deduced from paleosol sequences (e.g. Hatté et al., 2001; Gocke et al., 2014), which are abundant in East Africa due to the high rate of volcanic activity (e.g. in the Rungwe volcanic province, Fontijn et al., 2010). First applications of br GDGTs in such soil settings from across the world have revealed promising results (e.g. Peterse et al., 2011; Zech et al., 2012).

5. Conclusions

δ^2H_{wax} and br GDGT distributions were determined in 60 surface soils collected along altitudinal transects of two East African mountains (Mt. Rungwe in Tanzania and Mt. Kenya in Kenya). The obtained values were combined with data from altitudinal gradients of previous studies in the region to assess the applicability of integrated δ^2H_{wax}

and br GDGTs data sets as coupled paleo-topography and paleo-temperature proxies, respectively, in East Africa. Variations in δ^2H_{wax} do not systematically document altitudinal changes, with only one out of the three investigated mountains showing a positive relationship – even though the altitude effect was present in the δ^2H of precipitation. At the regional (East African) scale, coupling of estimated and observed δ^2H_p data highlights their spatial heterogeneity. The use of δ^2H_{wax} as a paleo-elevation proxy must therefore be restricted to site (mountain)-specific studies. In contrast, br GDGT-derived MAAT reliably track measured MAAT gradients along the four studied mountains (Mts Rungwe, Kenya, Kilimanjaro and Rwenzori). The large dataset of both measured and br GDGT-derived MAAT in the study area enabled to establish a new regional East African soil calibration between br GDGT distribution and MAAT. This new calibration improves the accuracy of MAAT reconstruction for the studied region, in comparison to other global soil calibrations, and highlights the potential of br GDGTs as paleo-thermometers in recent and ancient East African soils.

Acknowledgements

The authors would like to thank the RESON (Rungwe Environmental Science Observatory Network) and those who help them during field trips, notably Stephen Kajula, Winne Mosena, Matokeo Arbogast, Stephen Warui, Marcel Hale and the inhabitants of Masoko. Paul Donohoe and Bernard Bowler are warmly acknowledged for their technical support at Newcastle University. The authors are indebted to Dr. Pierre Camberlin (University of Bourgogne, France) who shared his temperature dataset from Mt. Kenya. This research benefited from a travel grant awarded by the EAOG and a PhD

scholarship from UPMC to S. Coffinet as well as support from the EC2CO program (CNRS/INSU) to A. Huguet. The work under permit NCST/RCD/17/013/02 on Mt. Kenya (C. Omuombo) was supported from French AIRD and Campus France through the French embassy in Nairobi.

References:

Anderson V.J., Shanahan T.M., Saylor J.E., Horton B.K., Mora A.R. (2014). Sources of local and regional variability in the MBT′/CBT paleotemperature proxy: Insights from a modern elevation transect across the Eastern Cordillera of Colombia. *Org. Geochem.* **69**, 42–51.

Araguás-Araguás L., Froehlich K., Rozanski K. (2000). Deuterium and oxygen-18 isotope composition of precipitation and atmospheric moisture. *Hydrol. Process.* **14**, 1341–1355.

Bai Y., Fang X., Jia G., Sun J., Wen R., Ye Y. (2015). Different altitude effect of leaf wax n-alkane δD values in surface soils along two vapor transport pathways, southeastern Tibetan Plateau. *Geochim. Cosmochim. Acta* **170**, 94–107.

Bremond L., Alexandre A., Wooller M.J., Hély C., Williamson D., Schäfer P.A., Majule A., Guiot J. (2008). Phytolith indices as proxies of grass subfamilies on East African tropical mountains. *Global Planet. Change* **61**, 209–224.

Bowen G. J. (2016) The Online Isotopes in Precipitation Calculator, version 2.2. http://www.waterisotopes.org.

Bowen, G. J., and Wilkinson B. (2002), Spatial distribution of $\delta^{18}O$ in meteoric precipitation, *Geology* **30**, 315–318.

Bowen G.J. and Revenaugh J. (2003). Interpolating the isotopic composition of modern meteoric precipitation. *Water Resour. Res.* **39**, 1299.

Camberlin P., Boyard-Micheau J., Philippon N., Baron C., Leclerc C., Mwongera C. (2014). Climatic gradients along the windward slopes of Mount Kenya and their implication for crop risks. Part 1: climate variability. *Int. J. Climatol.* **34**, 2136–2152.

Chikaraishi Y. and Naraoka H. (2007). $\delta^{13}C$ and δD relationships among three n-alkyl compound classes (n-alkanoic acid, n-alkane and n-alkanol) of terrestrial higher plants. *Org. Geochem.* **38**, 198–215.

Coffinet, S., Huguet, A., Williamson, D., Fosse, C., Derenne, S., 2014. Potential of GDGTs as a temperature proxy along an altitudinal transect at Mount Rungwe (Tanzania). *Org. Geochem.* **68**, 82–89.

Coffinet S., Huguet A., Williamson D., Bergonzini L., Anquetil C., Majule A., Derenne S. (2015). Occurrence and distribution of glycerol dialkanol diethers and glycerol

526 dialkyl glycerol tetraethers in a peat core from SW Tanzania. *Org. Geochem.* **83–**
527 **84**, 170–177.
528 Dang X., Yang H., Naafs D.A., Pancost R.D., Xie S., 2016. Evidence of moisture control
529 on the methylation of branched glycerol dialkyl glycerol tetraethers in semi-arid
530 and arid soils. *Geochim. Cosmochim. Acta* **189**, 24-36.
531 Dansgaard W. (1964). Stable isotopes in precipitation. *Tellus XVI* **4**, 436-468.
532 Delalande M., Bergonzini L., Massault M. (2008). Mbaka lakes isotopic (^{18}O and ^{2}H) and
533 water balances: discussion on the used atmospheric moisture compositions. *Isot*
534 *Environ Healt. S.* **44**, 71–82.
535 Dirghangi S.S., Pagani M., Hren M.T., Tipple B.J. (2013). Distribution of glycerol
536 dialkyl glycerol tetraethers in soils from two environmental transects in the USA.
537 *Org. Geochem.* **59**, 49–60.
538 Eglinton G. and Hamilton R.J. (1967). Leaf epicuticular waxes. *Science, New Series* **156**,
539 1322–1335.
540 Eglinton T.I. and Eglinton G. (2008). Molecular proxies for paleoclimatology. *Earth*
541 *Planet. Sc. Lett.* **275**, 1–16.
542 Ernst N., Peterse F., Breitenbach S.F.M., Syiemlieh H.J., Eglinton T.I. (2013).
543 Biomarkers record environmental changes along an altitudinal transect in the
544 wettest place on Earth. *Org. Geochem.* **60**, 93-99.
545 Fontijn K., Ernst G.G.J., Elburg M.A., Williamson D., Abdallah E., Kwelwa S., Mbede
546 E., Jacobs P. (2010). Holocene explosive eruptions in the Rungwe Volcanic
547 Province, Tanzania. *J. Volcanol. Geoth. Res.* **196**, 91–110.
548 Gocke M., Hambach U., Eckmeier E., Schwark L., Zöller L., Fuchs M., Löscher M.,
549 Wiesenberg G.L.B. (2014). Introducing an improved multi-proxy approach for
550 paleoenvironmental reconstruction of loess–paleosol archives applied on the Late
551 Pleistocene Nussloch sequence (SW Germany). *Palaeogeogr. Palaeoclimatol.*
552 *Palaeoecol.* **410**, 300–315.
553 Gonfiantini R., Roche M.-A., Olivry J.-C., Fontes J.-C., Zuppi G.M. (2001). The altitude
554 effect on the isotopic composition of tropical rains. *Chem. Geol.* **181**, 147–167.
555 Grab, S.W. (2013). Fine-scale variations of near-surface-temperature lapse rates in the
556 high Drakensberg escarpment, South Africa: environmental implications. *Arct.*
557 *Antarct. Alp. Res.* **45**, 500–514.
558 Hatté C., Antoine P., Fontugne M., Lang A., Rousseau D.-D., Zöller L. (2001). $\delta^{13}C$ of
559 Loess Organic Matter as a Potential Proxy for Paleoprecipitation. *Quaternary Res.*
560 **55**, 33–38.
561 Hijmans R.J., Cameron S.E., Parra J.L., Jones P.G., Jarvis A. (2005). Very high
562 resolution interpolated climate surfaces for global land areas. *Int. J. Climatol.* **25**,
563 1965–1978.
564 Hren M.T., Pagani M., Erwin D.M., Brandon M. (2010). Biomarker reconstruction of the
565 early Eocene paleotopography and paleoclimate of the northern Sierra Nevada.
566 *Geology* **38**, 7–10.
567 Huguet C., Hopmans E.C., Febo-Ayala W., Thompson D.H. Sinninghe Damsté J.S.,
568 Schouten S. (2006). An improved method to determine the absolute abundance of
569 glycerol dibiphytanyl glycerol tetraether lipids. *Org. Geochem.* **37**, 1036–1041.

570 Huguet, A., Fosse, C., Laggoun-Défarge, F., Toussaint, M.-L., Derenne, S. (2010).
571 Occurrence and distribution of glycerol dialkyl glycerol tetraethers in a French
572 peat bog. *Org. Geochem.* **41**, 559–572.
573 Jia G., Wei K., Chen F., Peng P. (2008). Soil n-alkane δD vs. altitude gradients along
574 Mount Gongga, China. *Geochim. Cosmochim. Acta* **72**, 5165–5174.
575 Kenya Meteorological Department, 1984: Climatological statistics for Kenya. KMD,
576 Nairobi, 87 p.
577 Loomis S.E., Russell J.M., Sinninghe Damsté J.S. (2011). Distributions of branched
578 GDGTs in soils and lake sediments from western Uganda: Implications for a
579 lacustrine paleothermometer. *Org. Geochem.* **42**, 739–751.
580 Luo P., Peng P. 'an, Gleixner G., Zheng Z., Pang Z., Ding Z. (2011). Empirical
581 relationship between leaf wax n-alkane δD and altitude in the Wuyi, Shennongjia
582 and Tianshan Mountains, China: Implications for paleoaltimetry. *Earth Planet.*
583 *Sc. Lett.* **301**, 285–296.
584 Macgregor D. (2015). History of the development of the East African Rift System: A
585 series of interpreted maps through time. *J. Afr. Earth Sci.* **101**, 232–252.
586 Menges J., Huguet C., Alcañiz J.M., Fietz S., Sachse D., Rosell-Melé A. (2014).
587 Influence of water availability in the distributions of branched glycerol dialkyl
588 glycerol tetraether in soils of the Iberian Peninsula. *Biogeosciences* **11**, 2571–
589 2581.
590 Nivet, F., Bergonzini, L., Diemer, L., Mathé, P.-E., Kajula, S., Ngingo, P., Mwasomba,
591 A., Noret, A., Majule, A., Williamson, D. (2015). RESON: 3-year records of
592 rainfall isotopic composition from 3 stations of the Rungwe volcanic province
593 (SW Tanzania). Presented at *Tropical deserts and lakes through time,*
594 *Paleohydrology, Isotope geochemistry, Climate and Societies*, Aix-en-Provence
595 (France).
596 Pedentchouk N., Sumner W., Tipple B., Pagani M. (2008). $\delta^{13}C$ and δD compositions of
597 n-alkanes from modern angiosperms and conifers: An experimental set up in
598 central Washington State, USA. *Org. Geochem.* **39**, 1066–1071.
599 Peterse F., van der Meer M.T.J., Schouten S., Jia G., Ossebaar J., Blokker J., Sinninghe
600 Damsté J.S. (2009). Assessment of soil n-alkane delta D and branched tetraether
601 membrane lipid distributions as tools for paleoelevation reconstruction.
602 *Biogeosciences* **6**, 2799–2807.
603 Peterse F., Prins M.A., Beets C.J., Troelstra S.R., Zheng H., Gu Z., Schouten S.,
604 Sinninghe Damsté J.S. (2011). Decoupled warming and monsoon precipitation in
605 East Asia over the last deglaciation. *Earth Planet. Sc. Lett.* **301**, 256–264.
606 Peterse F., van der Meer J., Schouten S., Weijers J.W.H., Fierer N., Jackson R.B., Kim J.-
607 H., Sinninghe Damsté J.S. (2012). Revised calibration of the MBT–CBT
608 paleotemperature proxy based on branched tetraether membrane lipids in surface
609 soils. *Geochim. Cosmochim. Acta* **96**, 215–229.
610 Rieti-Shati M., Yam R., Karlen W, Shemesh A. (2000). Stable isotope composition of
611 tropical high-altitude fresh-waters on Mt. Kenya, Equatorial East Africa. *Chem*
612 *Geol* **166**, 341-350.
613 Rolland, C. (2003). Spatial and Seasonal Variations of Air Temperature Lapse Rates in
614 Alpine Regions. *J. Climate* **16**, 1032–1046.

615 Sachse D., Billault I., Bowen G.J., Chikaraishi Y., Dawson T.E., Feakins S.J., Freeman
616 K.H., Magill C.R., McInerney F.A., van der Meer M.T.J., Polissar P., Robins R.J.,
617 Sachs J.P., Schmidt H.-L., Sessions A.L., White J.W.C., West J.B., Kahmen A.
618 (2012). Molecular Paleohydrology: Interpreting the Hydrogen-Isotopic
619 Composition of Lipid Biomarkers from Photosynthesizing Organisms. *Annu. Rev.*
620 *Earth Pl. Sc.* **40**, 221–249.
621 Sauer P.E., Eglinton T.I., Hayes J.M., Schimmelmann A., Sessions A.L. (2001).
622 Compound-specific D/H ratios of lipid biomarkers from sediments as a proxy for
623 environmental and climatic conditions. *Geochim. Cosmochim. Acta* **65**, 213–222.
624 Schimmelmann A., Sessions A.L., Mastalerz M. (2006). Hydrogen Isotopic (D/H)
625 Composition of Organic Matter During Diagenesis and Thermal Maturation.
626 *Annu. Rev. Earth Pl. Sc.* **34**, 501–533.
627 Schouten S., Hopmans E.C., Sinninghe Damsté J.S. (2013). The organic geochemistry of
628 glycerol dialkyl glycerol tetraether lipids: A review. *Org. Geochem.* **54**, 19–61.
629 Sepulchre P., Ramstein G., Fluteau F., Schuster M., Tiercelin J.-J., Brunet M. (2006).
630 Tectonic Uplift and Eastern Africa Aridification. *Science, New Series* **313**, 1419–
631 1423.
632 Sinninghe Damsté J.S., Ossebaar J., Schouten S., Verschuren D. (2008). Altitudinal shifts
633 in the branched tetraether lipid distribution in soil from Mt. Kilimanjaro
634 (Tanzania): Implications for the MBT/CBT continental palaeothermometer. *Org.*
635 *Geochem.* **39**, 1072–1076.
636 Sinninghe Damsté J.S., Ossebaar J., Schouten S., Verschuren D. (2012). Distribution of
637 tetraether lipids in the 25-ka sedimentary record of Lake Challa: extracting
638 reliable TEX_{86} and MBT/CBT palaeotemperatures from an equatorial African
639 lake. *Quaternary Sci. Rev.* **50**, 43–54.
640 Soderberg K., Good S.P., O'Connor M., Wang L., Ryan K., Caylor K.K. (2013). Using
641 atmospheric trajectories to model the isotopic composition of rainfall in central
642 Kenya. *Ecosphere* **4**, 1–18.
643 Smith, M. (1993). CLIMWAT for CROPWAT: A climatic database for irrigation
644 planning and management (No. FAO IDP-49). FAO, Roma (Italia).
645 Agrometeorological Group.
646 Tierney J.E., Russell J.M., Eggermont H., Hopmans E.C., Verschuren D., Sinninghe
647 Damsté J.S. (2010). Environmental controls on branched tetraether lipid
648 distributions in tropical East African lake sediments. *Geochim. Cosmochim. Acta*
649 **74**, 4902–4918.
650 Verschuren D., Sinninghe Damsté J.S., Moernaut J., Kristen I., Blaauw M., Fagot M.,
651 Haug G.H., Geel B. van, Batist M.D., Barker P., Vuille M., Conley D.J., Olago
652 D.O., Milne I., Plessen B., Eggermont H., Wolff C., Hurrell E., Ossebaar J.,
653 Lyaruu A., Plicht J. van der, Cumming B.F., Brauer A., Rucina S.M., Russell
654 J.M., Keppens E., Hus J., Bradley R.S., Leng M., Mingram J., Nowaczyk N.R.
655 (2009). Half-precessional dynamics of monsoon rainfall near the East African
656 Equator. *Nature* **462**, 637–641.
657 Vincens A., Williamson D., Thevenon F., Taieb M., Buchet G., Decobert M., Thouveny
658 N. (2003). Pollen-based vegetation changes in southern Tanzania during the last
659 4200 years: climate change and/or human impact. *Palaeogeogr. Palaeoclimatol.*
660 *Palaeoecol.* **198**, 321–334.

661 Weijers J.W.H., Schouten S., van den Donker J.C., Hopmans E.C., Sinninghe Damsté
662 J.S. (2007). Environmental controls on bacterial tetraether membrane lipid
663 distribution in soils. *Geochim. Cosmochim. Acta* **71**, 703–713.
664 West, A.G., February, E.C., Bowen, G.J. (2014). Spatial analysis of hydrogen and oxygen
665 stable isotopes ("isoscapes") in ground water and tap water across South Africa. *J.*
666 *Geochem. Explor.* **145**, 213–222.
667 Williamson D., Majule A., Delalande M., Mwakisunga B., Mathé P.-E., Gwambene B.,
668 Bergonzini L. (2014). A potential feedback between landuse and climate in the
669 Rungwe tropical highland stresses a critical environmental research challenge.
670 *Curr. Opin. Environ. Sustain.* **6**, 116–122.
671 Zech M., Zech R., Rozanski K., Gleixner G., Zech W. (2015). Do n-alkane biomarkers in
672 soils/sediments reflect the δ2H isotopic composition of precipitation? A case
673 study from Mt. Kilimanjaro and implications for paleoaltimetry and paleoclimate
674 research. *Isot Environ Healt. S.* **51**, 508–524.
675 Zech R., Gao L., Tarozo R., Huang Y. (2012). Branched glycerol dialkyl glycerol
676 tetraethers in Pleistocene loess-paleosol sequences: Three case studies. *Org.*
677 *Geochem.* **53**, 38–44.
678 Zhuang G., Pagani M., Chamberlin C., Strong D., Vandergoes M. (2015). Altitudinal
679 shift in stable hydrogen isotopes and microbial tetraether distribution in soils from
680 the Southern Alps, NZ: Implications for paleoclimatology and paleoaltimetry.
681 *Org. Geochem.* **79**, 56–64.

Figure captions

Fig. 1. Map of East Africa. The different sites mentioned in this study are represented with a star. A zoom-in is made for Mt. Kenya and Mt. Rungwe, the 2 sites specifically investigated in this study, and altitudinal profiles of the corresponding transects are shown.

Fig. 2. δ^2H_p estimations from the OIPC (the Online Isotopes in Precipitation Calculator; Bowen, 2016; Bowen and Revenaugh, 2003) along Mt. Rungwe, Tanzania (red segment), Mt. Kenya, Kenya (green segment) and Mt. Kilimanjaro, Tanzania (blue segment) together with on field δ^2H_p measurements along Mt. Kilimanjaro (blue circles; Zech et al., 2015) and Mt. Rungwe (red diamonds; Nivet et al. 2015). Note that the delimitations of each segment corresponds to the altitudinal range of the sample set investigated in the present study for each mount.

Fig. 3. δ^2H_{wax} values (A) along the altitudinal transects at Mt. Kenya, Kenya and (B) along the altitudinal transect at Mt Rungwe, Tanzania.

Fig. 4. Measured mean annual air temperature (MAAT) along altitudinal gradients in East Africa: Mt Rungwe (red diamonds; Coffinet et al., 2014); Mt. Kenya (green triangles; Camberlin et al., 2014), Mt. Rwenzori (purple squares; Loomis et al., 2011), Mt. Kilimanjaro (blue circles; Sinninghe Damsté et al., 2008)

Fig. 5. Comparison of the accuracy and precision of (A) the global soil MBT'/CBT calibration (Peterse et al., 2012) and (B) the new East African regional MBT'/CBT calibration developed in this study, the 1:1 line being represented in dashed grey as a reference. Application of these 2 calibrations to reconstruct br GDGT-derived MAAT variation with altitude in East Africa: (C) the global soil calibration (Peterse et al., 2012), (D) the new East African soil calibration where the black solid line is the derived linear regression obtained from br GDGT-derived MAAT and the dashed black line is the measured MAAT altitudinal gradient (as obtained in Fig. 3). Colours correspond to each mountain of the region: Mt Rungwe (red diamonds; Mt. Rungwe, this study and Coffinet et al., 2014); Mt. Kenya (green triangles; this study), Mt. Rwenzori (purple squares; Loomis et al., 2011), Mt. Kilimanjaro (blue circles; Sinninghe Damsté et al., 2008);

Table 1. Weighted average δ^2H of C_{27}, C_{29} and C_{31} *n*-alkanes (denoted δ^2H_{wax}) together with br GDGT-derived mean annual air temperature (MAAT) from Peterse et al. (2012) calibration and from the regional calibration developed in this study.

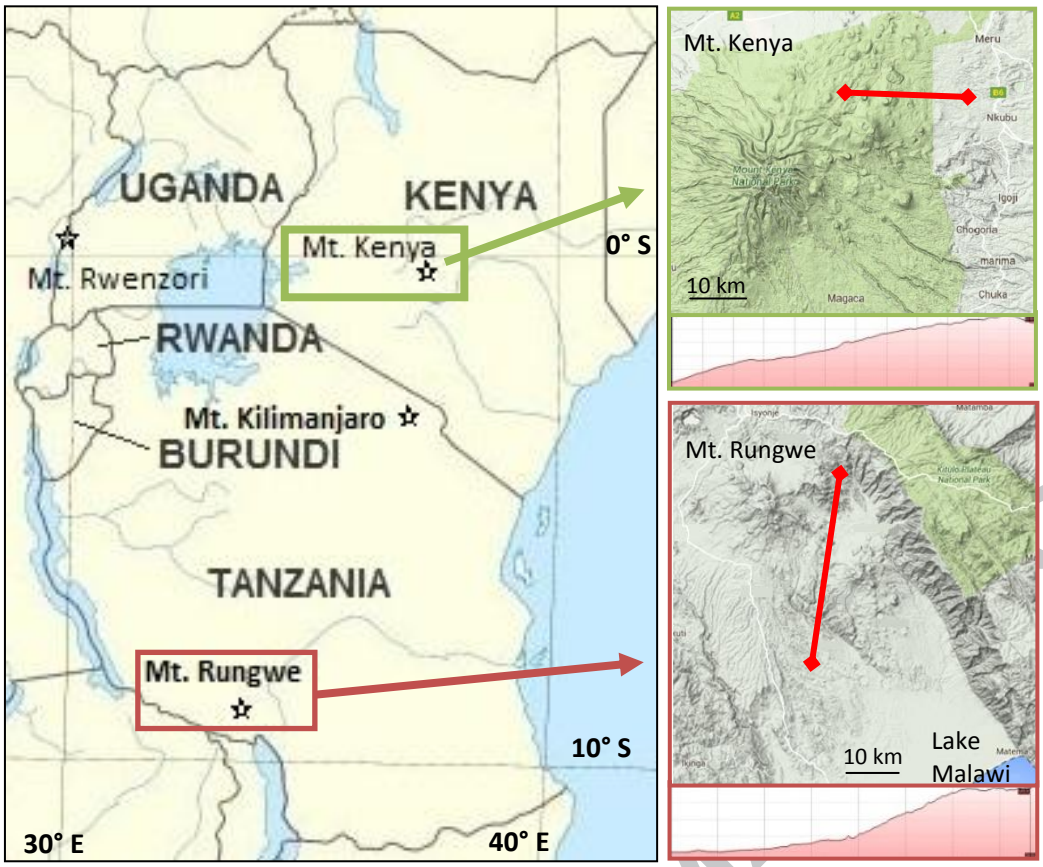

Figure 1.

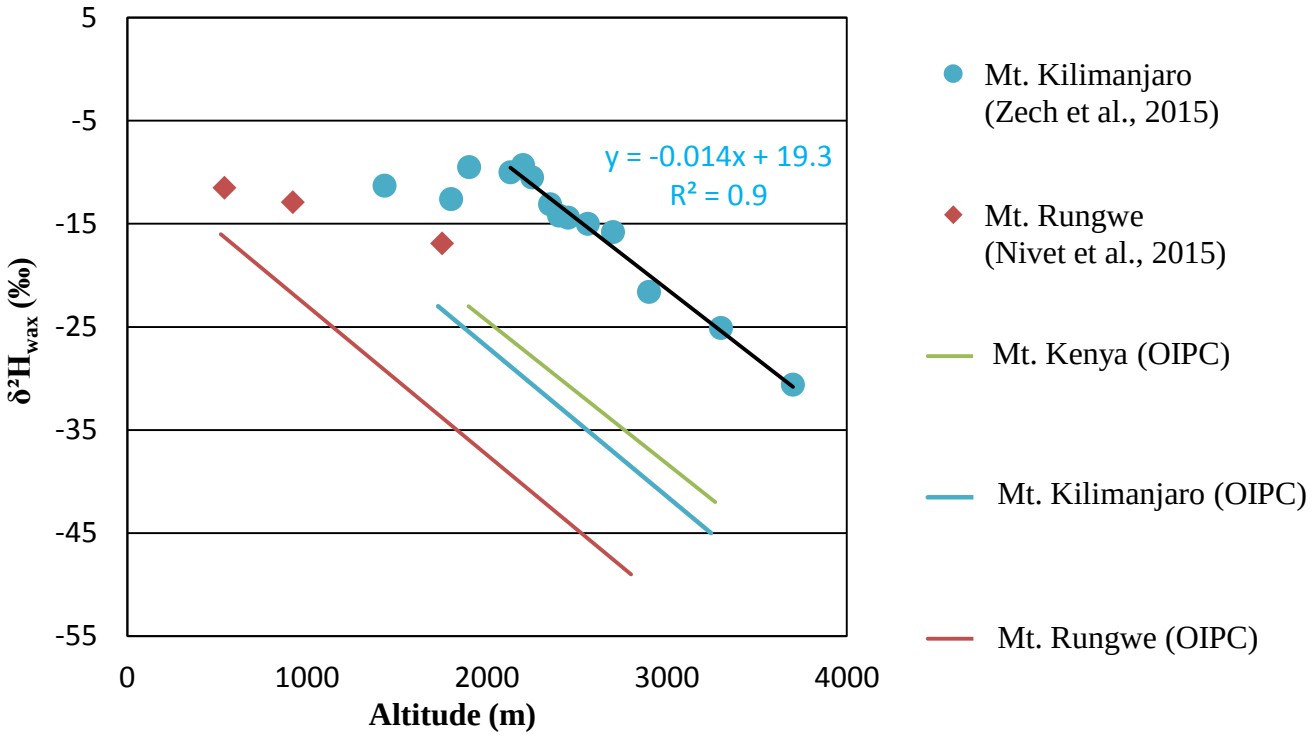
5
-5
-15
-25
-35
-45
-55
0
1000
2000
3000
4000
Altitude (m)
δ²H_wax (‰)
y = -0.014x + 19.3
R² = 0.9
Mt. Kilimanjaro (Zech et al., 2015)
Mt. Rungwe (Nivet et al., 2015)
Mt. Kenya (OIPC)
Mt. Kilimanjaro (OIPC)
Mt. Rungwe (OIPC)

Figure 2.

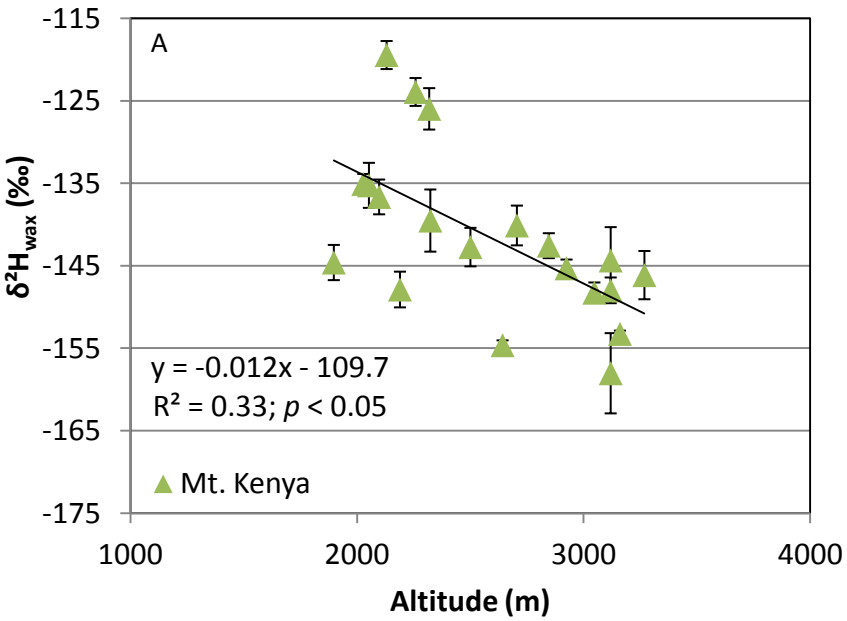

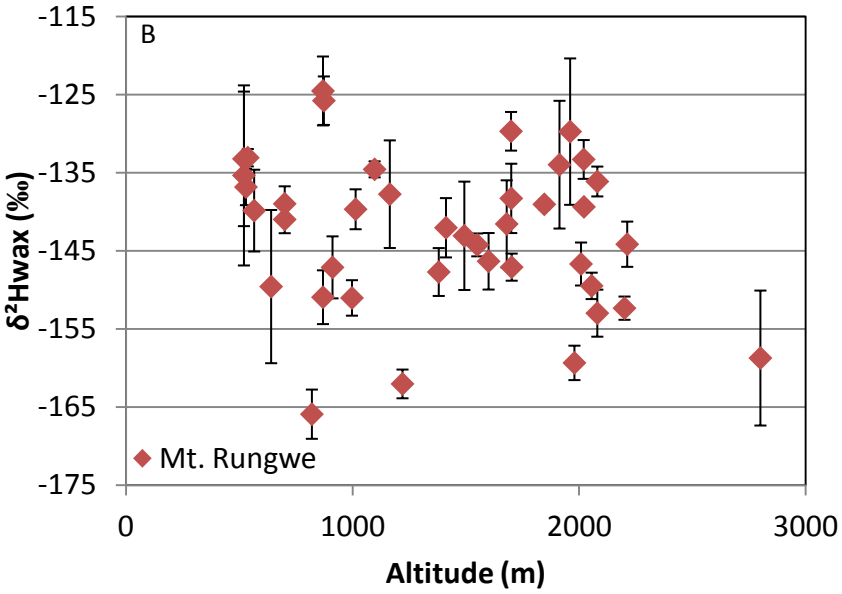

Figure 3.

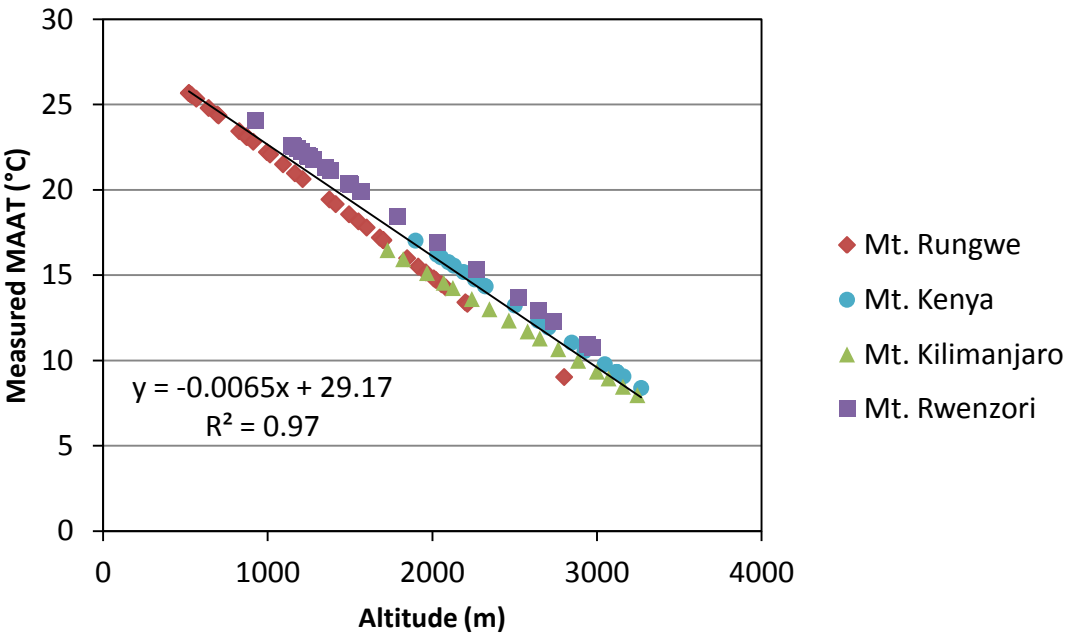

Figure 4.

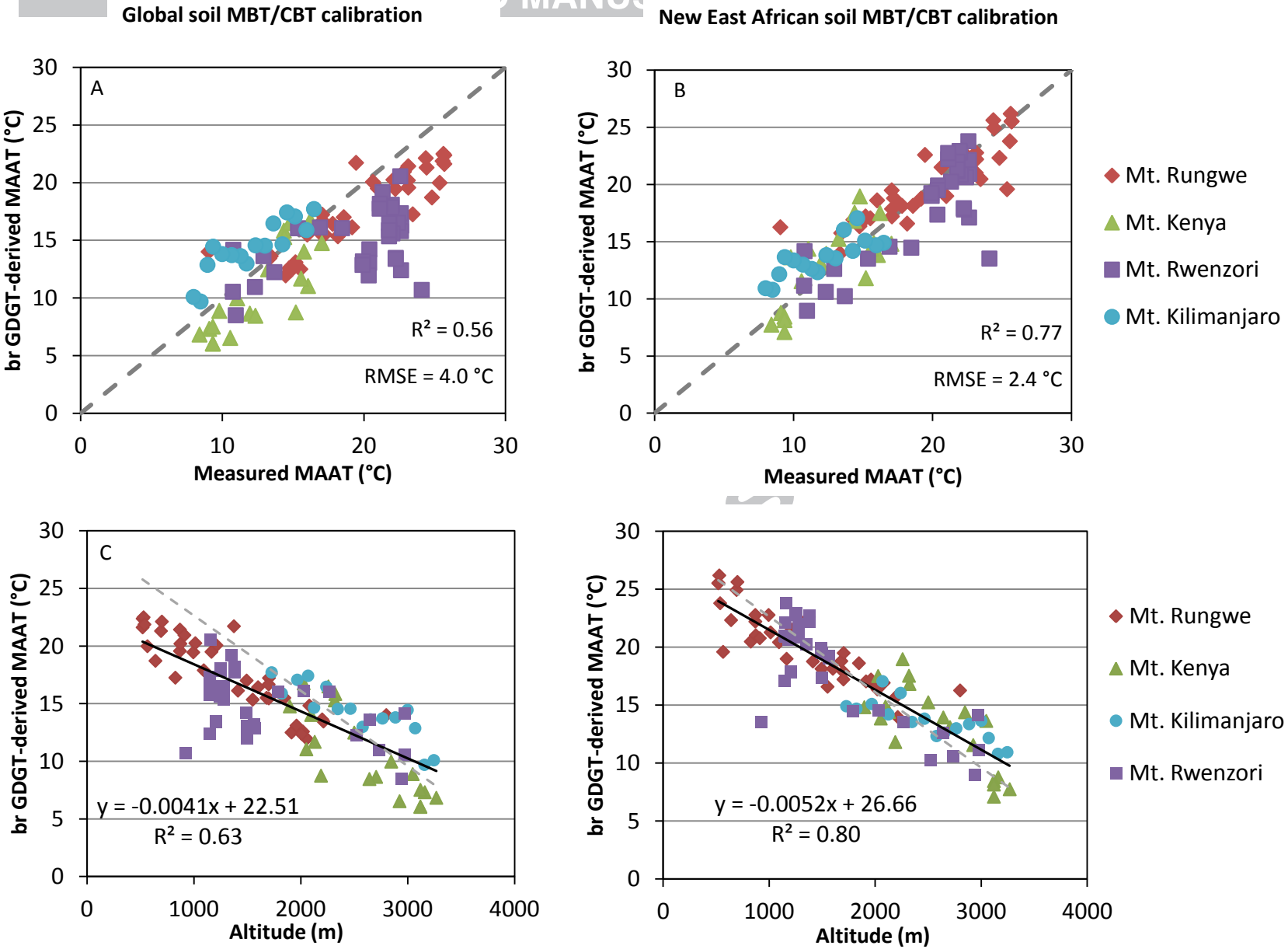

Figure 5.

Table 1.

camp.	n°	altitude (m.a.s.l.)	MAAT (Peterse et al.. 2012)	MAAT (this study)	δ^2H_{wax} [a] (‰)	camp.	n°	altitude (m.a.s.l.)	MAAT (Peterse et al.. 2012)	MAAT (this study)	δ^2H_{wax} (‰)	camp.	n°	altitude (m.a.s.l.)	MAAT (Peterse et al.. 2012)	MAAT (this study)	δ^2H_{wax} (‰)
Mt. Rungwe (2012)	1	520	21.6	25.9	-133±9	Mt. Rungwe (2014)	22	537	21.9	24.5	-133±1	Mt. Kenya (2013)	41	3160	10.0	9.6	-153±0
	2	520	22.4	26.0	-135±12		23	565	20.0	20.8	-140±5		42	3119	10.2	9.4	-148±2
	3	529	22.5	26.6	-137±2		24	700	22.1	26.1	-141±2		43	3119	10.2	8.9	-158±5
	4	640	18.7	22.8	-150±10		25	873	20.2	22.0	-126±3		44	3119	10.2	8.1	-144±4
	5	700	21.3	25.4	-139±2		26	911	20.9	21.9	-147±4		45	3268	9.3	8.7	-146±3
	6	820	17.3	21.0	-166±3		27	1013	20.2	22.2	-140±3		46	3047	10.3	13.9	-148±1
	7	869	19.6	22.8	-151±3		28	1164	19.5	20.2	-138±7		47	2924	11.7	11.8	-145±1
	8	869	21.4	23.6	-125±4		29	1412	16.1	19.4	-142±4		48	2846	11.9	14.7	-143±2
	9	997	19.5	23.3	-151±2		30	1493	17.0	19.0	-143±7		49	2705	13.0	13.4	-140±2
	10	1097	17.9	21.1	-135±1		31	1600	16.4	18.9	-146±4		50	2642	13.2	14.1	-155±1
	11	1220	20.1	22.3	-162±2		32	1699	16.7	18.8	-130±2		51	2500	13.8	15.9	-143±2
	12	1380	21.7	23.5	-148±3		33	1700	15.5	18.0	-138±4		52	2323	14.7	17.8	-140±4
	13	1550	15.4	17.5	-144±1		34	1913	12.5	17.3	-134±8		53	2189	15.5	12.4	-148±2
	14	1680	15.5	19.3	-142±6		35	1960	13.1	17.6	-130±9		54	2097	16.2	15.8	-137±2
	15	1702	17.2	20.2	-147±2		36	2008	12.4	17.0	-147±3		55	2052	16.4	14.5	-135±3
	16	1846	15.5	19.2	-139±1		37	2212	13.5	15.0	-144±3		56	1897	16.9	15.9	-145±2
	17	2020	12.8	16.8	-133±2		38	2080	n.a.[b]	n.a.	-136±2		57	2027	16.4	18.5	-135±1
	18	2055	12.2	17.1	-149±2		39	2021	n. a.	n.a.	-139±0		58	2130	15.8	15.0	-119±2
	19	2080	14.8	17.7	-153±1		40	1979	n.a.	n.a.	-159±2		59	2258	15.1	19.6	-124±2
	20	2200	13.6	16.5	-152±1								60	2318	14.9	18.2	-126±3
	21	2800	14.0	17.0	-159±9												

[a] the analytical error of at least duplicate measurements is given

[b] not analysed for GDGT content.